



Evidence for extended acceleration of solar flare ions from 1–8 MeV solar neutrons detected with the MESSENGER Neutron Spectrometer

William C. Feldman,¹ David J. Lawrence,² John O. Goldsten,² Robert E. Gold,² Daniel N. Baker,³ Dennis K. Haggerty,² George C. Ho,² Säm Krucker,⁴ Robert P. Lin,^{4,5} Richard A. Mewaldt,⁶ Ronald J. Murphy,⁷ Larry R. Nittler,⁸ Edgar A. Rhodes,² James A. Slavin,⁹ Sean C. Solomon,⁸ Richard D. Starr,¹⁰ Faith Vilas,¹¹ and Angelos Vourlidas⁶

Received 5 June 2009; revised 9 September 2009; accepted 18 September 2009; published 23 January 2010.

[1] Neutrons produced on the Sun during the M2 flare on 31 December 2007 were observed at 0.48 AU by the MESSENGER Neutron Spectrometer. These observations are the first detection of solar neutrons inside 1 AU. This flare contained multiple acceleration episodes as seen in type III radio bursts. After these bursts ended, both the energetic particle and neutron fluxes decayed smoothly to background with an e -folding decay time of 2.84 h, spanning a 9 h time period. This time is considerably longer than the mean lifetime of a neutron, which indicates that either the observed neutrons were generated in the spacecraft by solar energetic particle protons, or they originated on the Sun. If most of the neutrons came from the Sun, as our simulations of neutron production on the spacecraft show, they must have been continuously produced. A likely explanation of their long duration is that energetic ions were accelerated over an extended time period onto closed magnetic arcades above the corona and then slowly pitch angle-scattered by coronal turbulence into their chromospheric loss cones. Because of their relatively low energy loss in the Neutron Spectrometer (0.5–7.5 MeV), most of these neutrons beta decay to energetic protons and electrons close to the Sun, thereby forming an extended seed population available for further acceleration by subsequent shocks driven by coronal mass ejections in interplanetary space.

Citation: Feldman, W. C., et al. (2010), Evidence for extended acceleration of solar flare ions from 1–8 MeV solar neutrons detected with the MESSENGER Neutron Spectrometer, *J. Geophys. Res.*, 115, A01102, doi:10.1029/2009JA014535.

1. Introduction

[2] Understanding the mechanisms of energetic-particle acceleration has long been a goal of space physics. Despite much progress since the space-flight era began, many gaps in our knowledge remain. One of the largest of these

involves energetic-ion acceleration in solar flares. These ions are difficult to detect remotely if they do not have access to magnetic field lines that connect the corona to interplanetary space, a common outcome because 90% of all ions accelerated in a compilation of impulsive flares [see *Hua and Lingenfelter*, 1987, Figure 17] remain tied to the Sun on closed magnetic field lines. Whereas energetic electrons can be imaged relatively easily through their bremsstrahlung and gyrosynchrotron radiation, energetic ions are visible only through their coupling to gamma rays and/or neutrons, which are relatively difficult to detect.

[3] Several recent studies [e.g., *Miller et al.*, 1997; *Hua et al.*, 2002; *Murphy et al.*, 2007] have shown that combined analyses of gamma rays and neutrons from solar flares are essential to constrain adequately the many parameters needed to account for the total number, energy spectrum, time dependence, and angular distribution of all ions accelerated. Such a combined analysis is also essential for constraining our understanding of the magnetic and plasma structure of the flare neighborhood in the corona. This structure controls the acceleration, trapping, and transport of energetic ions.

[4] Stemming from the limitation to date on measuring neutrons at 1 AU, many more flares have been observed in

¹Planetary Science Institute, Tucson, Arizona, USA.

²Johns Hopkins University Applied Physics Laboratory, Laurel, Maryland, USA.

³Laboratory for Atmospheric and Space Physics, University of Colorado, Boulder, Colorado, USA.

⁴Space Sciences Laboratory, Physics Department, University of California, Berkeley, California, USA.

⁵School of Space Research, Kyung Hee University, Yongin, Geonggi, Korea.

⁶Physics Department, California Institute of Technology, Pasadena, California, USA.

⁷Naval Research Laboratory, Washington, D. C., USA.

⁸Department of Terrestrial Magnetism, Carnegie Institution of Washington, Washington, D. C., USA.

⁹NASA Goddard Space Flight Center, Greenbelt, Maryland, USA.

¹⁰Department of Physics, Catholic University of America, Washington, D. C., USA.

¹¹MMT Observatory, University of Arizona, Tucson, Arizona, USA.

gamma rays than in neutrons. At 1 AU, the flux of fast neutrons having energies near their production maximum (\sim a few MeV) in the corona will be very low as a consequence of the finite neutron lifetime (mean lifetime = 886 s; see *Nieto et al.* [2008]). This circumstance has limited joint neutron and gamma-ray analyses to flares having large impulsive phases. For the most part, flares amenable to such analyses have necessarily been large, and all previous neutron detections have been at energies above about 20 MeV [see *Ryan*, 2000, and references therein].

[5] At present, the Reuven Ramaty High-Energy Solar Spectroscopic Imager (RHESSI) spacecraft [*Lin et al.*, 2002] provides the most comprehensive source of high-energy X-ray and gamma-ray data that are suitable for studies of ion acceleration in solar flares. Solar flare neutrons have for some time been, and are currently, monitored by ground-based neutron detectors [*Ryan*, 2000]. The only source of solar neutron data from space at present is the Neutron Spectrometer (NS) sensor of the Gamma-Ray and Neutron Spectrometer (GRNS) instrument [*Goldsten et al.*, 2007] on the Mercury Surface, Space Environment, Geochemistry, and Ranging (MESSENGER) spacecraft [*Solomon et al.*, 2007]. This spacecraft is presently orbiting the Sun between 0.30 AU and 0.63 AU en route to orbit insertion about Mercury in March 2011. Between now and then, the aphelion of MESSENGER's orbit will continuously decrease from its present 0.63 AU to that of the aphelion of Mercury, 0.45 AU. Its orbit about Mercury is presently scheduled to last one Earth year.

[6] A drawing of the MESSENGER spacecraft showing the locations of the NS sensor of GRNS relative to spacecraft structures is shown in Figure 1a. The locations of other MESSENGER instruments and sensors that figure importantly in the analysis of this event, such as the X-Ray Spectrometer (XRS) solar monitor, Magnetometer, and Energetic Particle Spectrometer (EPS), are also shown. A drawing of the NS and a schematic representation of its three sensor components are given in Figures 1b and 1c. The spacecraft is actively oriented so that the sunshade always points toward the Sun.

[7] The MESSENGER NS is sufficiently sensitive to solar neutrons as to complement the measurements of solar flare gamma rays that are now provided by RHESSI. The energy range of the NS for fast neutrons (apparent deposited energies between 0.5 and 7.5 MeV) covers the maximum flux portion of solar flare neutrons at the top of the corona simulated by *Murphy et al.* [2007]. The MESSENGER NS therefore provides a new window on solar neutron production that will span the rise from minimum to maximum solar activity during solar cycle 24.

[8] To date, the MESSENGER NS has sampled neutrons from the Venus atmosphere once, the surface of Mercury twice, and galactic cosmic ray (GCR) interactions with spacecraft material during the cruise phase of the mission between aphelia near 0.7 AU and several perihelion passages at 0.30–0.33 AU. We have therefore been able to check its performance, develop a model of the spacecraft structure, which defines quantitatively the generation of fast neutrons by GCRs, solar energetic particle (SEP) protons, as well as the field of view of the NS, and estimate the sensor's capability to detect and analyze fast neutrons from the Sun. A realistic test for this capability was afforded through

observation of the M2 solar flare (as observed using the MESSENGER XRS) that began at 0043 UTC on 31 December 2007.

[9] This paper summarizes those MESSENGER observations of the 31 December 2007 flare and offers an assessment of some of their implications. A brief overview of the flare as observed by (1) RHESSI in hard X-rays, (2) Solar Terrestrial Relations Observatory (STEREO) A and B in extreme ultraviolet (EUV), (3) Geostationary Operational Environmental Satellites (GOES) in soft X-rays, and (4) the Bruny Island Radio Spectrometer (BIRS) in Australia [*Erickson*, 1997] and the STEREO B Radio Spectrometer in radio waves is given in section 2. The observations made by MESSENGER instruments of X-rays, energetic electrons, the interplanetary magnetic field (IMF), and neutrons are given in section 3. Simulations of the NS response to neutrons generated locally in the spacecraft from the spacecraft response to energetic protons that may have been present during the time of enhanced neutron detection by the NS are given in section 4. A discussion of the importance of this event in constraining solar flare ion acceleration, trapping, and transport in the corona is given in section 5. Our findings are limited by the fact that the flare occurred at 102°E longitude relative to Earth, and so gamma rays from the impulsive phase of this flare were not seen by RHESSI. In addition, the energetic particle detector aboard MESSENGER was not fully operational so we have no definitive measure of the energetic proton environment at the time of enhanced neutron detection.

2. The 31 December 2007 Solar Flare as Seen by GOES, RHESSI, STEREO, and BIRS

[10] The 31 December 2007 solar flare was observed by many different instruments aboard several spacecraft at different longitudes around the Sun. Data for the part of the flare visible above the limb observed by GOES in soft X-rays with a magnitude of C8, by RHESSI in both soft and hard X-rays, and by both STEREO A and B in EUV [*Howard et al.*, 2008], are shown in Figure 2. The flare site was at 102°E from the Earth-Sun line and so was beyond the eastern limb of the Sun from STEREO A, GOES, and RHESSI. Nevertheless, STEREO A was able to image a well-formed coronal mass ejection (CME) lifting off of the eastern limb at 0048:30 UTC [*Liu et al.*, 2009], and both GOES and RHESSI were able to observe the soft and hard X-ray emission from hot coronal loops that rose above the limb as the flare progressed. During the peak of the event, RHESSI also detected nonthermal X-ray emission originating from the corona (Figure 2) (*S. Krucker et al.*, Measurements of the coronal acceleration region of a solar flare, submitted to *Astrophysics Journal*, 2009). The non-thermal emission is unusually intense compared with other partially disk-occulted flares [*Krucker and Lin*, 2008] and comes from above the thermal flare loops, similar to that seen in the Masuda flare (see Figure 2) [*Masuda et al.*, 1994]. Gamma rays, which are predominantly produced low in the atmosphere, were not detected by RHESSI. We also note that an image of the Sun in EUV by the Extreme Ultraviolet Imager (EUVI) on STEREO B showed a classic two-ribbon structure.

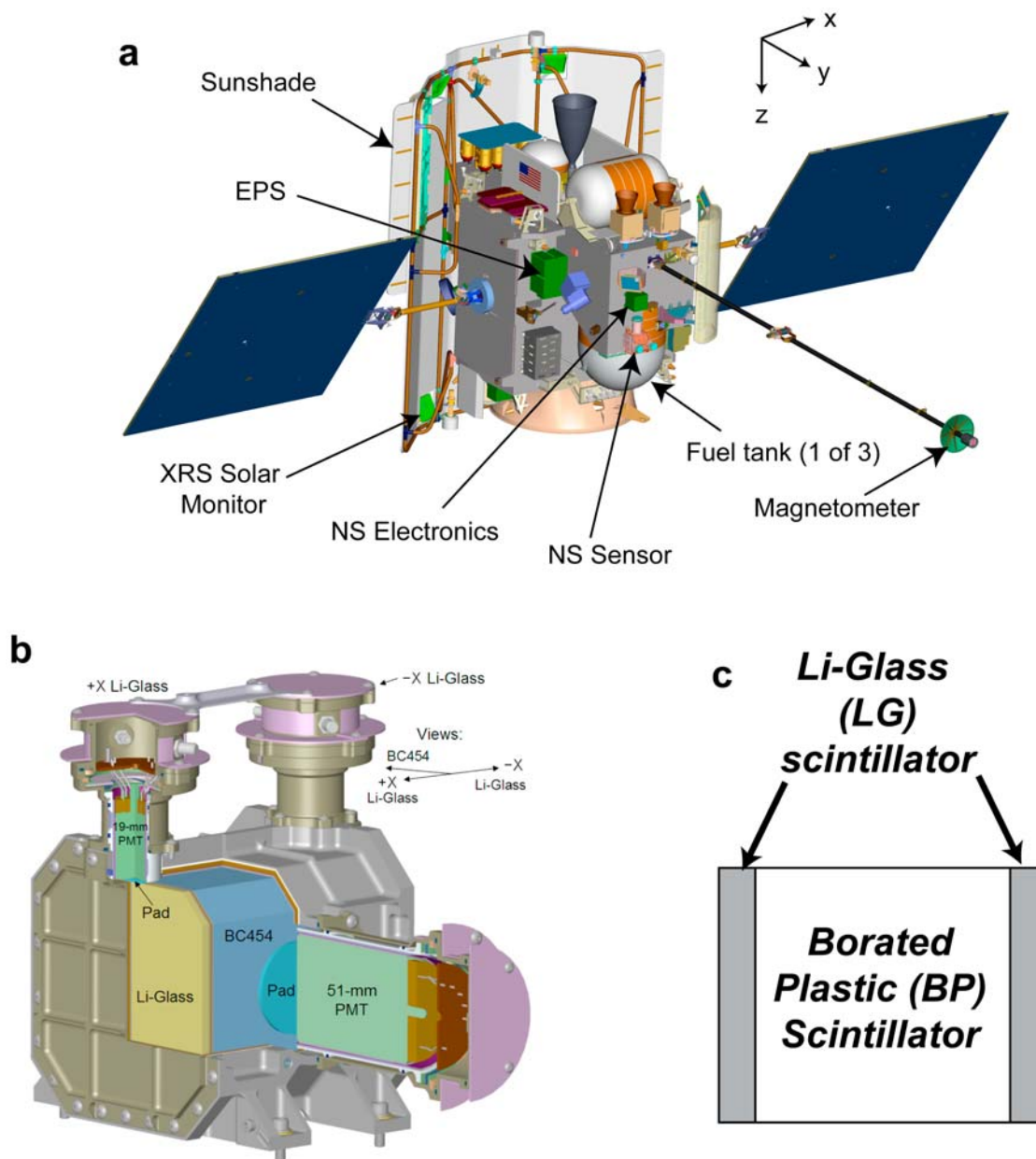


Figure 1. (a) Engineering drawing of the MESSENGER spacecraft [Leary *et al.*, 2007] showing the locations of the Neutron Spectrometer (NS sensor), X-Ray Spectrometer (XRS) solar monitor, Magnetometer, and Energetic Particle Spectrometer (EPS) sensor relative to the sunshade at left and the three intervening fuel tanks that shield the NS from the Sun. (b) Engineering drawing of the MESSENGER NS and a simplified schematic of the placement of the three NS sensor components. BC454 in Figure 1b refers to the designation of (c) the borated plastic scintillator.

[11] Both multiple type II and type III radio bursts were observed with the radio spectrometers aboard STEREO B [Bougeret *et al.*, 2008] and at BIRS [Erickson, 1997], as shown in Figure 3 [Liu *et al.*, 2009]. All of these events in the low and intermediate corona extended from about 0052 to about 0120 UTC on 31 December 2007. While the several type III events indicate multiple, discrete electron-acceleration events in the corona, the type II radiation indicates that the CME and/or explosively driven compressive waves in the corona were traveling sufficiently fast

relative to the ambient solar wind plasma close to the Sun that they were able to drive shock waves. The longitudinal extent of these shocks is not known.

3. Observations by MESSENGER

[12] At the time of the solar flare in question, MESSENGER was at about 0.48 AU and 153°E relative to the Earth-Sun line. Instruments aboard MESSENGER observed the flare through its signatures in 1–8 keV X-rays [Schlemm *et*

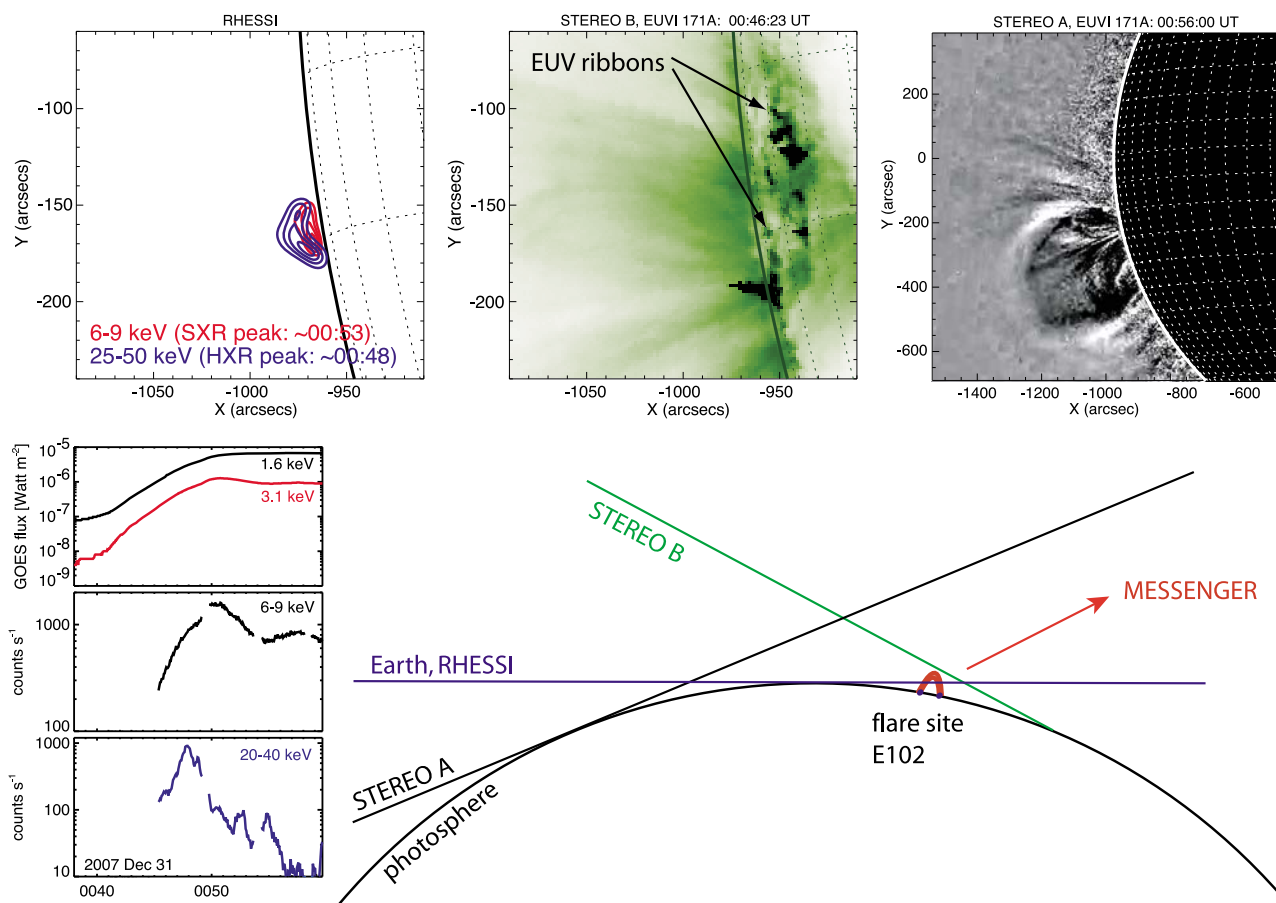


Figure 2. A pictorial overview of the major events associated with the 31 December 2007 solar flare as seen by the RHESSI, GOES, and STEREO A/B spacecraft. Their respective heliographic observation perspectives are shown at the lower right. GOES and RHESSI observed soft X-ray (SXR) and hard X-ray (HXR) emission from just beyond the eastern limb. The EUVI on STEREO B imaged a two-ribbon structure, and STEREO A showed a CME lift-off above the eastern solar limb, as seen from its heliographic perspective.

al., 2007], electrons (and perhaps some ions) at energies between 65 keV and 1 MeV [Andrews *et al.*, 2007], characteristic variations in the IMF [Anderson *et al.*, 2007], and neutrons having apparent energies deposited in the NS between 0 and 7.5 MeV [Goldsten *et al.*, 2007]. No measurements of gamma rays are available during the 31 December 2007 event because the MESSENGER GRS was not turned on at the time. The XRS solar monitor views the Sun through a small aperture in the Sun-facing sunshade, the EPS sensor has a fan-shaped field of view ($\pm 80^\circ$ latitude by $\pm 6^\circ$ longitude) centered on the anti-Sun line, the Magnetometer is on a 3.6 m boom in the antisunward direction to isolate it from spacecraft magnetic fields, and the NS is on the back of the spacecraft bus with a view of the Sun through two large fuel tanks containing N_2H_4 and one fuel tank containing N_2O_4 [Leary *et al.*, 2007], as shown in Figure 1a. The fuel load at the time of the flare was sufficient to cause significant neutron scattering and energy moderation. Preliminary simulations [Lawrence *et al.*, 2009] using a model of the spacecraft as input to the Monte Carlo particle transport code, MCNPX [Pelowitz, 2005], indicate that the spacecraft materials are sufficiently massive to soften considerably and attenuate the energy

spectrum of neutrons from the Sun. They are also sufficiently massive to generate fast neutrons from SEP protons if the flux of these protons above 30 MeV is sufficiently high. Details of these simulations, including quantitative estimates of potential SEP-produced neutron counting rates on the NS, are given in section 4.

[13] The NS is composed of three separate sensors that span the apparent neutron energy range between 0 and about 7.5 MeV [Goldsten *et al.*, 2007], as shown in Figures 1b and 1c. It consists of a sandwich of two square lithium-glass (LG) plates (+XLG and -XLG) that bracket a cubical block of borated plastic (BP) scintillator. The LG sensors are 10 cm by 10 cm in area and 4 mm thick, with their normals pointed at right angles to the spacecraft-Sun line ($-Y$ direction). The BP scintillator is 10 cm on a side. The LG sensors are sensitive to both thermal and epithermal neutrons (energies between 0 and about 100 keV), and the BP sensor is sensitive to epithermal and fast neutrons (total electronic energy range between about 1 eV and 7.5 MeV). As shown in Figure 1a, the sensor is mounted to one side of the back panel of the MESSENGER spacecraft. Accordingly, one of the LG sensors, +XLG, has its field of view cut in half by the spacecraft, and the other, -XLG, has a full 2π field of view

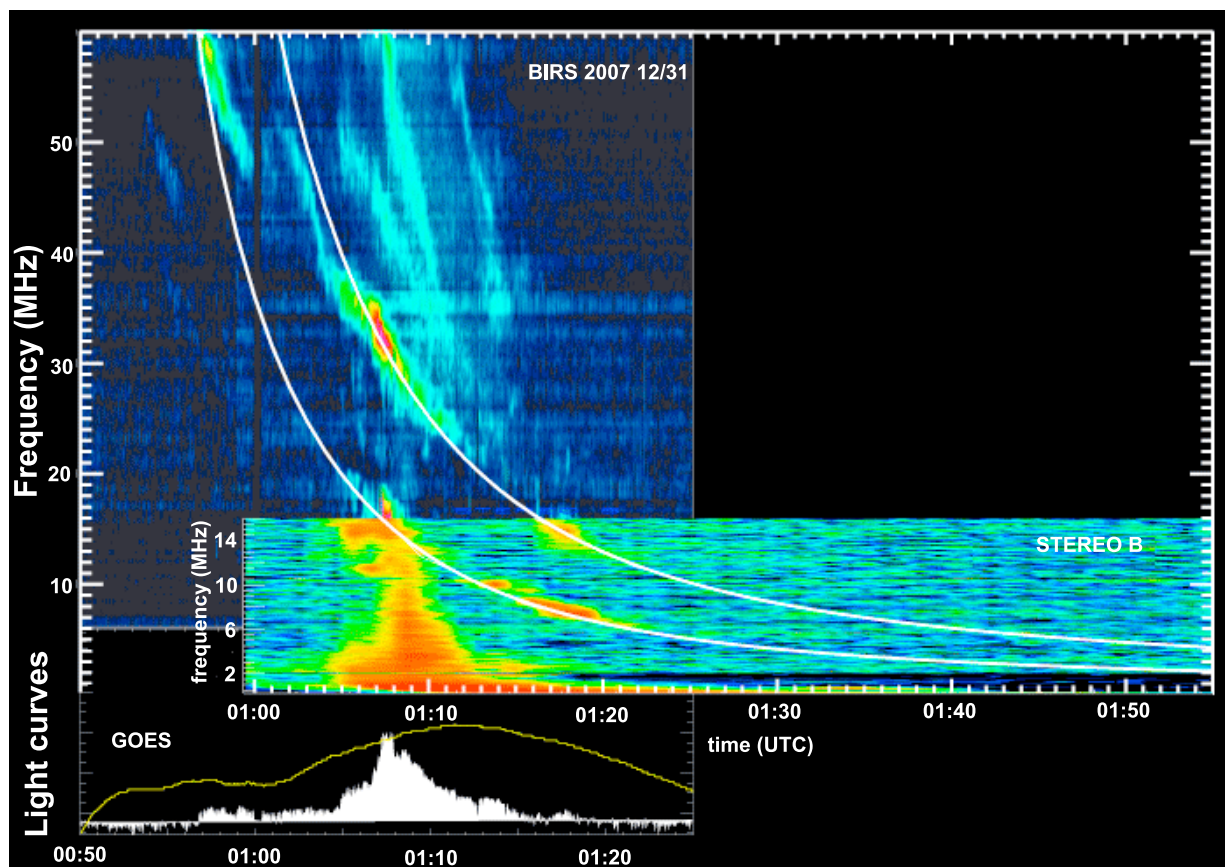


Figure 3. Radio spectrograms measured from BIRS between 17 and 60 MHz and from STEREO B between 1 and 16 MHz, showing multiple type III bursts and several short segments of type II bursts. Increasing radio flux intensity goes from dark blue to red. At the bottom are shown the 1–8 keV soft X-ray flux from GOES (yellow curve) and the sum over all radio emission frequencies (histogram plot).

of interplanetary space. In consequence, $-XLG$ has a field of view that is about twice that of $+XLG$. Except for brief periods, the NS has been operating continuously since February 2007.

[14] Counting rates registered by the XRS in soft X-rays at 300 s time intervals are shown in Figure 4a. The initial rise started at 0038 UTC and ended at about 0048 UTC. These times are about 7 min earlier than those observed by both GOES and RHESSI in soft and hard X-rays when all times are adjusted for light propagation from the Sun to 0.48 and 1 AU, respectively (Figure 2). Analysis of the X-ray energy spectrum measured by the MESSENGER XRS to determine the temperature and emission measure of the 31 December 2007 flare in 1–8 keV X-rays gives a flare magnitude of M2 when propagated to 1 AU.

[15] The initial rise of fast-neutron counting rates shown in Figure 4b began at about 0118 UTC. The abrupt termination of counts at about 0136 UTC is due to the BP being placed into a safe mode when its counting rate exceeded a preprogrammed upper limit.

[16] The time difference (Δt) between the two vertical lines in Figures 4a and 4b (after adding 240 s for the X-ray transit time from the Sun to MESSENGER) can be used to estimate the highest-energy neutron detected by the NS, $E_n(\text{max}) = 4.8 \pm 0.6$ MeV. This estimate is approximate

because without observation of the impulse as seen in gamma rays we do not know the time of initiation of high-energy ion acceleration in the corona. If we choose instead the initiation time of the largest of the type II radio bursts seen by BIRS at about 0056 UTC (see upper end of the leftmost white trace in Figure 3), we derive $E_n(\text{max}) = 8$ MeV after adding the 500 s transit time for the radio waves between the Sun and Earth.

[17] Energetic particles from the event arrived at the spacecraft at about 0120 UTC, as shown in Figures 5a and 5b, which display counting rates for three broad energy ranges spanning 65 keV to 1 MeV for the entire event. We note the nearly simultaneous, sharp rise from background to maximum intensity, with no measurable velocity dispersion. This enhancement in counting rates was observed by both the EPS detector looking radially away from the Sun and by the two LG plates looking at right angles to the Sun direction, as shown in Figures 4c and 5b. Inspection of all three counting rates shows: (1) general overall temporal agreement (within statistics); (2) that at early times the rates of $+XLG$ and $-XLG$ display multiple injection impulses in the corona and/or intermittent magnetic connection to the flare site; and (3) that the e -folding decay time between 0440 and 1000 UTC was 2.84 h.

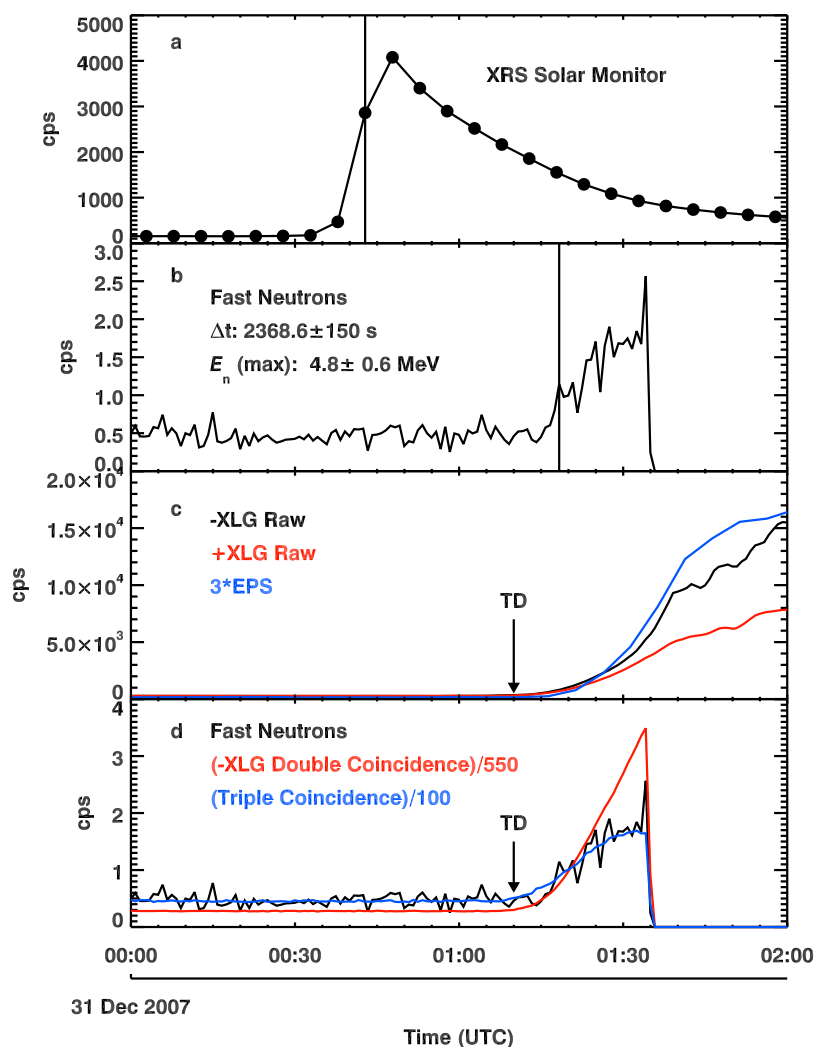


Figure 4. (a) Response of the XRS solar monitor to X-rays during the 31 December 2007 solar flare. (b) NS detector response to fast neutrons produced by the solar flare. (c) Rates of energetic particle counts at MESSENGER measured using the two Li-glass scintillators and the EPS detector; 260 s should be added to the time axis in Figure 4a to indicate when the event would have been seen at 1 AU if GOES could have viewed the solar disc. The EPS counting rates have been scaled by a factor of 3 to match that registered by the $-$ XLG scintillator. The two vertical lines in Figures 4a and 4c denote the start time of neutron generation in the corona (Figure 4a) and the earliest detection time of neutrons at the spacecraft (Figure 4b). (d) An overlay of fast-neutron, $-$ XLG double-coincidence, and $-$ XLG, BP, and $+$ XLG triple-coincidence counting rates before the BP data dropout. The triple-coincidence rate is normalized to the fast-neutron rate just before triggering the safe mode at about 0135 UTC, and the double-coincidence counting rates are normalized to the fast-neutron rate just after exit from the safe mode (see Figure 5c). TD denotes the arrival of a tangential discontinuity as seen in the Magnetometer record. The energy range of the EPS is 65 keV to 1.0 MeV; the energy range of the single raw LG counting rates for electrons is from 300 keV to about 2 MeV and protons up to about 30 MeV; the energy range of the double-coincidence rates for electrons is from about 2 to 20 MeV and protons from about 30 to 120 MeV; and the energy range for triple-coincidences of electrons is greater than about 20 MeV and protons greater than about 120 MeV.

[18] We note that because of a failure of the EPS micro-channel plate, the EPS cannot distinguish between electrons and ions in this energetic particle event. However, the first detection of the event at MESSENGER occurred nearly simultaneously with the neutron onset, at about 39.5 min after flare onset. In consequence, the counting rates recorded by the EPS (having energies <1 MeV; see Figure 5a) must

have been due entirely to electrons, because protons having the same energies as the detected electrons would have arrived at MESSENGER later than the first-arriving neutrons. This conclusion holds also for all energetic particles detected by the EPS before the data dropout at about 0135 UTC. Transit times between flare onset and the data dropout correspond to that for a 1.5 MeV proton, which is greater

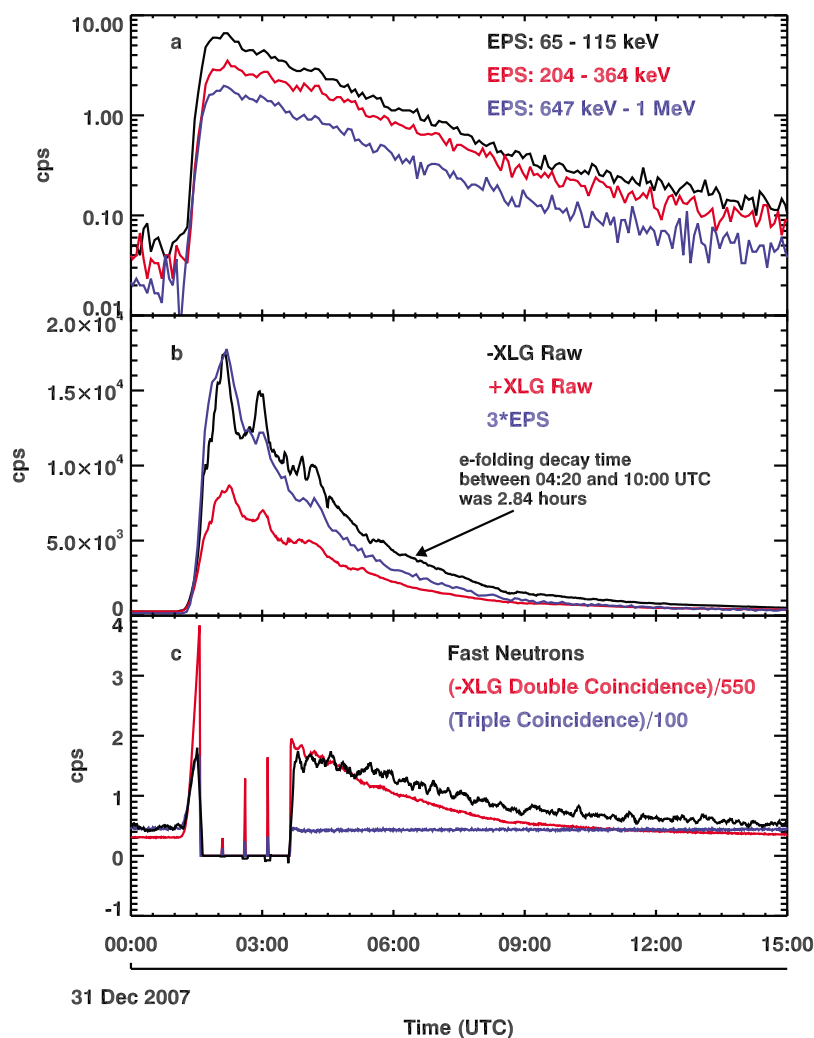


Figure 5. (a) Time-dependent counting rates of energetic electrons measured with the MESSENGER EPS detector. The top (black) curve is for 65 to 115 keV, the middle (red) curve is for 204 to 364 keV, and the bottom (blue) curve is for 647 keV to 1 MeV. (b) Rates of energetic particle counts at MESSENGER measured using the two Li-glass scintillators and the EPS detector. The EPS counting rates have been scaled to match that registered by the $-XLG$ scintillator. (c) An overlay of fast-neutron (black curve), $-XLG$ double-coincidence (red curve), and $-XLG$, BP, and $+XLG$ triple-coincidence (blue curve) counting rates throughout the entire fast-neutron event. The triple-coincidence rate is normalized to the fast-neutron rate just before triggering the safe mode at about 0135 UTC (shown in Figure 4b), and the double-coincidence counting rates are normalized to the fast-neutron rate just after exit from the safe mode. The three vertical lines during the safe mode record three failed attempts to exit the safe mode before the BP counting rate dropped below the preprogrammed safe level.

than the 1 MeV upper limit of the EPS in Figures 4c, 5a, and 5b. The smooth, monotonic decay with no inflection in counting rates for the 0.6–1 MeV channel of the EPS (the blue trace in Figure 5a) argues that any ion flux (which would have shown an ion velocity dispersion enhancement some time during the borated plastic dropout period) at the spacecraft during this entire event must have been completely overshadowed by the incident electron flux.

[19] The particle onset occurred just after a tangential discontinuity (TD) was observed in the Magnetometer data as shown in Figure 6 (and indicated by the vertical line in Figures 4c and 4d). As seen in Figure 6 there was a large enhancement in the magnitude of the magnetic field, B ,

starting at about 0820 UTC on 31 December 2007 (labeled SSI for stream-stream interaction region in Figure 6), and a smaller enhancement at about 0100 UTC on 1 January 2008 (labeled CME for coronal mass ejection in Figure 6). A close inspection of all magnetic field data during 31 December 2007 and 1 January 2008 revealed no shocks. We therefore deduce: (1) that the first rotational discontinuity separated neighboring magnetic flux tubes having different connection sites in the corona; (2) that the first large enhancement in B identified a density compression driven by a high-speed stream emanating from an open field region east of the flare site that corotated into the low-speed wind from the closed field region that preexisted above the flare site

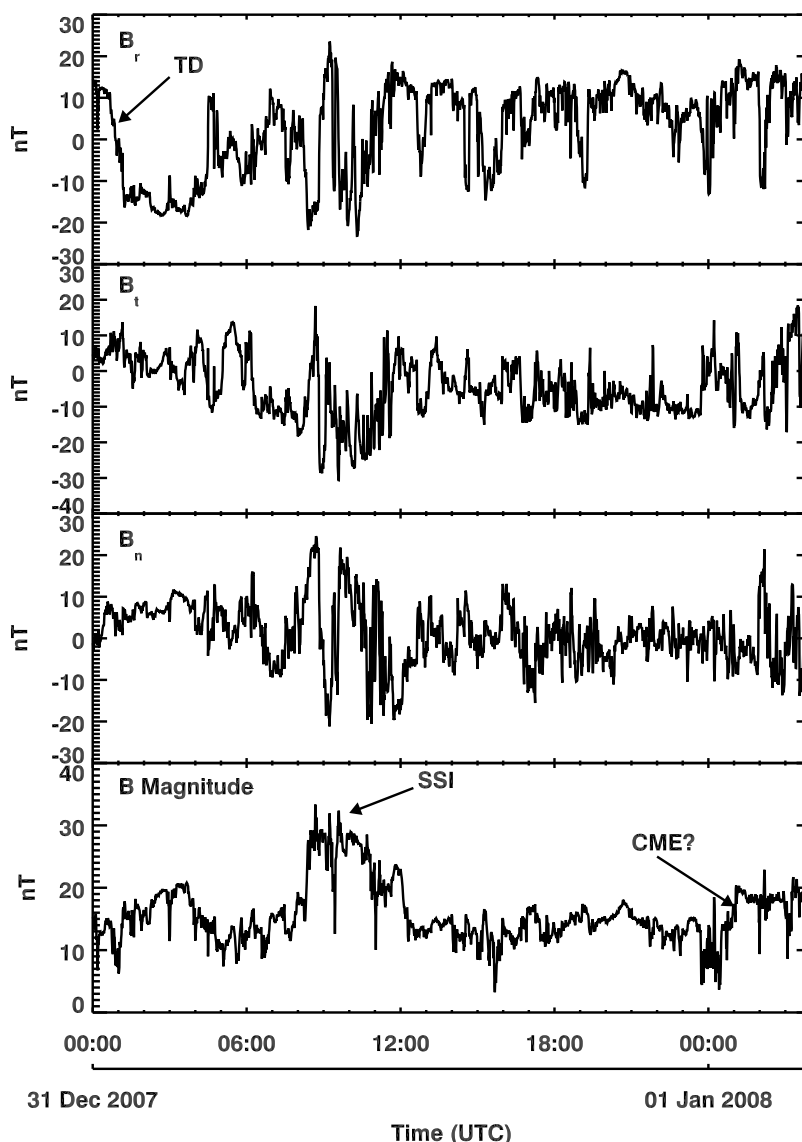


Figure 6. The time history of all three components and the magnitude of \mathbf{B} during 31 December 2007 and 1 January 2008. From top to bottom, they correspond to B_r , the radial component of \mathbf{B} ; B_t , the azimuthal component of \mathbf{B} ; and B_n , the component of \mathbf{B} normal to Mercury's orbital plane. TD, the arrival of a tangential discontinuity at 0112 UTC; SSI, a magnetic enhancement beginning at about 0820 UTC denoting the compression region of a stream-stream interaction region; CME, a magnetic enhancement beginning at about 0100 UTC on 1 January and perhaps signaling the arrival of the eastern flank of the CME at MESSENGER. No shock was observed during the entire 2-day period.

[Baker *et al.*, 2009]; and (3) that the second (much smaller increase in \mathbf{B}) enhancement at about 0100 UTC on 1 January 2008 perhaps signaled the passage of a small compression at the eastern flank of the CME released near the time of the flare. The timing of this second enhancement relative to the lift-off of the CME shown in Figure 2 gives an average speed from the Sun to MESSENGER of about 830 km/s. This speed is somewhat larger than that determined for the compression at the central longitude of the CME by the STEREO coronagraph, 780 km/s, or along the northeastern streamer at the flank of the CME, 620 km/s [Liu *et al.*, 2009]. All three speeds are comparable to, but slightly larger than, that predicted for the high-speed stream by the Baker *et al.*

[2009] model, about 600 km/s. Regardless, the speed difference between the CME and solar wind perpendicular to the compressive disturbance driven by the CME at its flank may have been sufficiently small as to be consistent with our lack of observation of a shock wave at the far eastern flank of the CME, which may have intersected the MESSENGER spacecraft.

[20] Our identification of the counting-rate enhancement seen by the BP scintillator starting at 0118 UTC as fast neutrons is demonstrated in Figure 7. The identification of fast neutrons by the BP sensor relies on detection of a characteristic double-interaction event [see Goldsten *et al.*, 2007, Figure 10]. The first interaction signifies the loss of

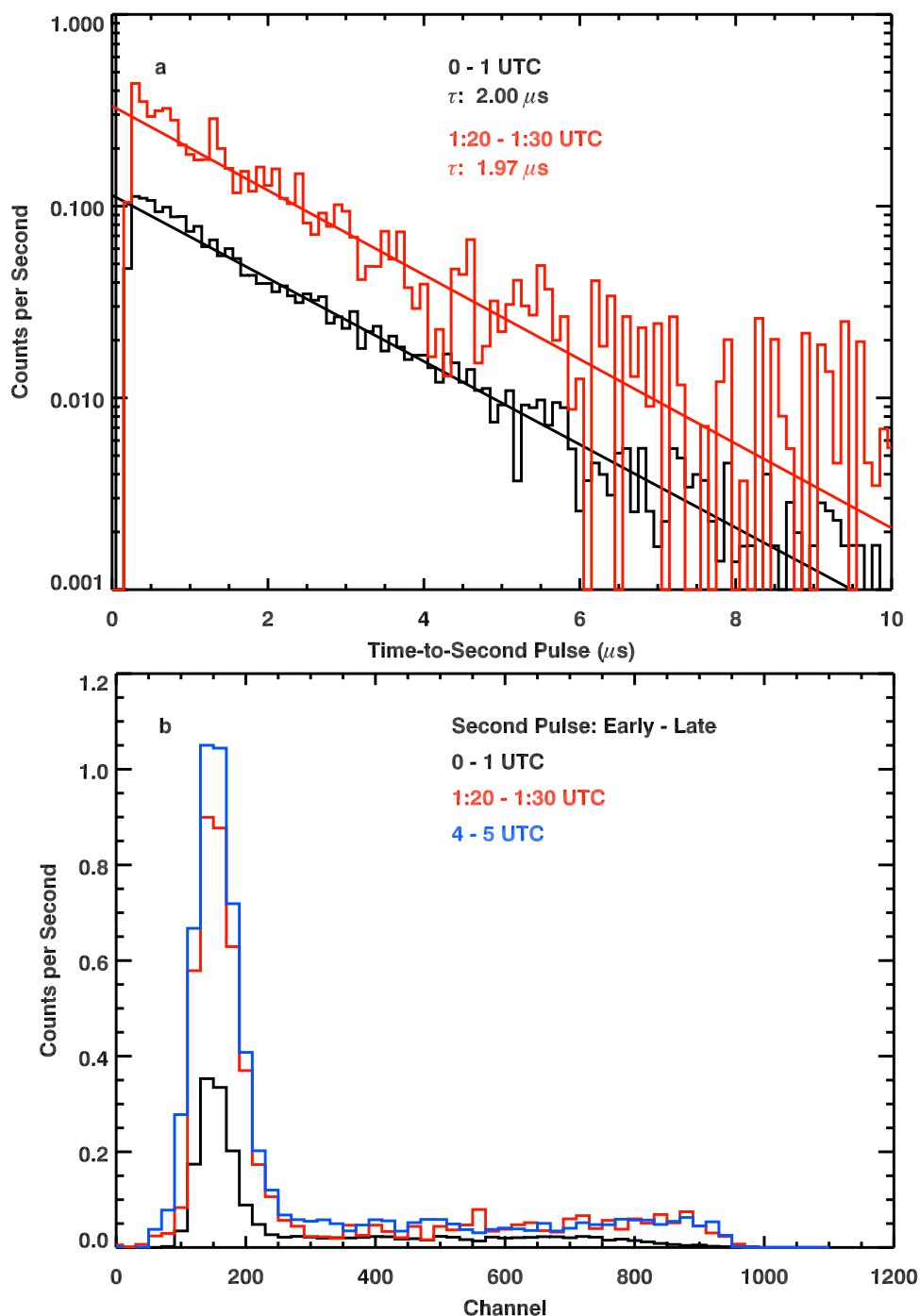


Figure 7. (a) Counting-rate histograms of the time to second pulses of two-interaction events measured before (black trace) and just after (red trace) the onset of enhanced fast-neutron counting rates. The straight lines show the expected $2.0 \mu\text{s}$ die away expected for the $^{10}\text{B}(n, \alpha)^7\text{Li}$ reaction. (b) An overlay of histograms of the pulse-height spectra of second interactions measured before the fast-neutron event (0000–0100 UTC), at early times during the event (0120–0130 UTC), and at late times during the event (0400–0500 UTC). The channel number is proportional to the energy deposited in the borated plastic scintillator during the second interaction.

all the neutron energy in the scintillator, and the second signifies the Q value (the excess energy in an exothermic reaction) of the $^{10}\text{B}(n, \alpha)^7\text{Li}$ reaction. The mean time separation between these two interactions in the MESSENGER sensor is about $2.0 \mu\text{s}$, fixed by the boron content of the

scintillator. Figure 7a shows histograms of time to second pulses after the chance coincidences measured between 20 and $25 \mu\text{s}$ have been subtracted (e.g., see Goldsten *et al.* [2007, Figure 10c] showing this subtraction). The black trace in Figure 7a shows data taken before the event when

only background fast neutrons owing to GCRs were present. The red trace in Figure 7a shows fast neutrons measured just after the initiation of the event. Both time periods show the characteristic exponential decay of about $2 \mu\text{s}$, which signifies the positive detection of neutrons. The characteristic response of the BP sensor to the $^{10}\text{B}(n,\alpha)^7\text{Li}$ reaction is shown in Figure 7b. Three pulse-height spectra are shown: one due to cosmic ray-generated neutrons in the spacecraft between 0000 and 0100 UTC, before the solar flare event, and the two others corresponding to observations during the event (before and after the BP sensor went into safe mode). All three spectra are identical in shape as required for their interpretation as signifying fast neutrons.

[21] Energetic particles are also measured using coincidence-counting rates in the NS, either through double coincidences between the BP and +XLG or -XLG sensors, or by triple coincidences among the BP and both LG sensors. Figures 4d and 5c show an overlay of fast-neutron counting rates (black lines) and NS-measured energetic particle counting rates (red lines (double) and blue lines (triple)). All rates were corrected for detector dead time, and the coincidence counting rates were additionally corrected for chance coincidences. The break in the counting rates between about 0136 and 0320 UTC in Figure 5c results from the safe mode. The three spikes in the middle of this dropout result from three failed attempts by the detector to exit from the safe mode. A close inspection (Figures 4d and 5c) shows that all three counting rates began their enhancements at about the same time (we believe that any apparent differences are not statistically significant). Also shown in Figure 4d is the time of passage of the tangential discontinuity. The triple-coincidence rates are scaled so that they align with the fast-neutron rates during the initial part of the event. However, when the safe mode ended, the triple rate had already fallen to its background level while the fast-neutron rate remained high (Figure 5c). We also note that the -XLG-BP double-coincidence rate rose to high values before entering the safe mode but then returned to rates that more nearly follow those of the fast neutrons after exiting the safe mode. The -XLG-BP-coincidence rate is scaled to the fast-neutron rates right after exiting the safe mode to facilitate the comparison. Although the fast-neutron and double-coincidence rates have generally similar relative time dependences just after exit from the safe mode, they are very different before the safe mode and have significant differences after about 0600 UTC as well.

[22] The general similarity between the EPS, -XLG-raw, double-coincidence, and triple-coincidence counting rates is no doubt because they are all responding to the same energetic-particle event. However, their dissimilarity during distinct parts of this event reflects the fact that they respond to different charged-particle energy ranges. The lowest range is covered by the EPS, 65 keV to 1.0 MeV; the next higher range is covered by the single raw LG counting rates, electrons from 300 keV to about 2 MeV or protons up to about 30 MeV; then comes the range of the double-coincidence rates, electrons from about 2 MeV to 20 MeV or protons from about 30 MeV to 120 MeV; and finally the triple-coincidence energy range corresponds to electrons at greater than about 20 MeV or protons at greater than about 120 MeV. That double- and triple-coincidence rates differ before and after the safe mode, as shown in Figure 5c,

indicates that the spectrum must soften and weaken with time during the event. We return to the implications of these observations in section 5.

4. Simulation of Spacecraft Response to Energetic Protons

[23] Although at this point we have no solid evidence for the detection at the MESSENGER spacecraft of protons having energies greater than 30 MeV (the threshold energy for the generation of secondary neutrons through interactions with spacecraft material), the possibility that such protons are present cannot be ruled out. We do know that most of the particles detected by the EPS between 65 keV and 1 MeV throughout the flare event must have been electrons. We may nonetheless estimate upper limits on the generation of secondary neutrons from interactions between primary SEP protons and spacecraft material that could have contributed to the fast-neutron counting rates shown in Figures 4d and 5c.

[24] Before presenting results of simulations of the spacecraft response to energetic SEP protons, we start with a quantitative understanding of the response of the NS on MESSENGER to GCRs. As noted in section 3, -XLG has an almost unblocked field of view at right angles to the spacecraft-Sun line, and +XLG faces in the opposite direction with half of its field of view cut off by the spacecraft. For the purpose of accounting for and understanding proton counting rates of GCR particles using the rates of double coincidences between the -XLG and BP scintillator, and the rates of triple coincidences at all three scintillators (-XLG, BP, and +XLG), we choose a coordinate system with the Z' axis aligned with the $-x$ axis in Figure 1, normal to the two LG plates and passing through their centers. This coordinate system is adopted for a cylindrically symmetric charged-particle telescope with two rectangular detectors in the work of *Sullivan* [1971, Figure 3]. Both plates have an area A of 100 cm^2 and are separated by 10 cm. The response of this type of detector to an isotropic particle flux having an intensity F_0 is $C = G F_0$, where C is the detector counting rate and G is a geometrical factor. G is given by *Sullivan* [1971, equation (11)], which for the triple-coincidence rate with the NS geometry simplifies to $G = 2(0.628)A$. Here, the factor of 2 is included to account for both directions coupling +XLG and -XLG. If we choose an isotropic GCR flux for solar minimum conditions of $F_0 = 4.4/(4\pi) \text{ cm}^{-2} \text{ s}^{-1} \text{ sr}^{-1}$ [e.g., *McKinney et al.*, 2006] then the triple-coincidence GCR counting rate is:

$$C(\text{triple}) = F_0 G = [4.4/(4\pi)](1.256)(100) = 44 \text{ s}^{-1}.$$

We measure $C(\text{triple}) = 43 \text{ s}^{-1}$.

[25] Additionally, the double-coincidence cosmic ray counting rate is given by:

$$\begin{aligned} C(\text{double}) &= C(\text{isotropic}) - C(\text{triple}) \\ &= (2\pi - 1.256)[4.4/(4\pi)](100) \\ &= 176 \text{ s}^{-1} \end{aligned}$$

We measure $C(\text{double}) = 165 \text{ s}^{-1}$. As a note in passing, the measured GCR double-coincidence cruise counting rate is

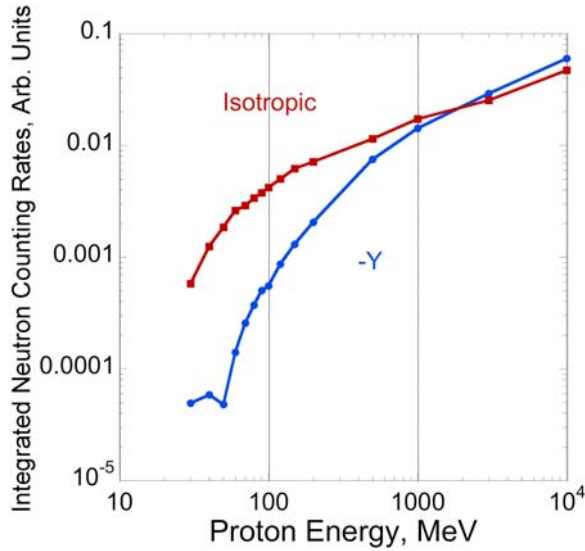


Figure 8. Energy dependence of fast neutrons that intercept the Neutron Spectrometer on MESSENGER between 0.5 and 7.5 MeV energy produced by the monoenergetic protons incident on the sunshade side of the spacecraft (blue curve) and isotropically (red curve).

the same within 2% if we use +XLG-BP or -XLG-BP coincidences. We conclude that the measured double- and triple-coincidence counting rates are close to what they should be for an average cosmic ray flux at solar minimum in interplanetary space near 1 AU.

[26] We can relate the measured neutron counting rates from energetic protons (either from GCRs or SEPs) by carrying out particle transport models of the MESSENGER spacecraft in a manner similar to what has been done for neutrons hitting the spacecraft [Lawrence *et al.*, 2009]. In particular, the geometry and materials have been modeled with the code MCNPX [Pelowitz, 2005]. These simulations consisted of plane waves of monoenergetic protons ranging in energy between 10 MeV and 10 GeV that are coming from the Sun (-Y), from the anti-Sun direction (+Y), and along the perpendicular to the spacecraft-Sun line ($\pm Z$). We assume that both the GCR and SEP proton spectra are isotropic at the location of the NS after the data dropout. We then determine the SEP-produced neutron counting rate by scaling the observed GCR-produced neutron counting rate by the ratio of simulated cosmic ray counting rates to our upper-limit estimate for SEP proton-generated neutron counting rates. We do this by normalizing the simulated neutron spectra at the NS for each proton energy simulation to one per cm^2 per second. We then convert these spectra to neutron counting rates using measured neutron detection efficiencies, which scale as $1/E_n$. These energy-dependent neutron-counting rates are then integrated between 0.5 MeV and 7.5 MeV, the range of energy sensitivity of the MESSENGER NS. We further assume that all energetic particles given by the double-coincidence rates in Figure 5c are due to protons, with none due to electrons. This assumption corresponds to a gross overestimate for the SEP-generated neutron estimate, which then provides an upper limit to the contribution from SEP protons to the fast-neutron counting rates in Figures 4d and 5c.

[27] The summed neutron counting rate $F_n(E_p)$ as a function of incident proton energy E_p is shown in Figure 8. The curve in blue gives $F_n(E_p)$ for protons incident from the sunward direction (-Y). The curve in red gives the average $F_n(E_p)$ under the assumption that the simulations are symmetric about the spacecraft-Sun direction,

$$F_{n,\text{avg}}(E_p) = \{F_{n,+Y}(E_p) + 2[F_{n,-Z}(E_p) + F_{n,+Z}(E_p)] + F_{n,-Y}(E_p)\}/6.$$

[28] The spectrum of GCRs was chosen from McKinney *et al.* [2006] for a solar modulation potential of 350 MV, characteristic of solar-minimum conditions, a potential that gives an isotropic GCR flux of $4.23/(4\pi) \text{ cm}^{-2} \text{ s}^{-1} \text{ sr}^{-1}$ for energies between 30 MeV and 10 GeV. This value is very close to the $4.4/(4\pi) \text{ cm}^{-2} \text{ s}^{-1} \text{ sr}^{-1}$ flux that agrees with our triple- and double-coincidence counting rates, as mentioned above. The energy spectrum of SEP proton intensity was chosen to correspond to that measured on 20 February 2002 during the largest impulsive SEP event seen at 1 AU during solar cycle 23 (see E. Chollet, J. Giacalone, and R. A. Mewaldt, Effects of interplanetary transport on the interpretation of solar energetic particle spectra and composition, manuscript in preparation, 2009). This spectrum was fit by the functional form:

$$dF/dE = K (E+0.12)^{-2.41} \exp(-E/62.5), \quad (1)$$

where K is a constant and all expressions for energy E are in MeV. For comparison purposes, we also chose a power law spectrum having an exponent of -3.5 , which was found by Lin *et al.* [2003] to agree with gamma-ray line ratios measured during the 23 July 2002 impulsive-flare event. All three proton spectra were normalized to a fluence of unity and are shown in Figure 9a. These spectra were then multiplied by $F_{n,\text{avg}}(E_p)$ to yield the neutron counting rates for energies between 0.5 MeV and 7.5 MeV shown in Figure 9b. Integrating over all proton energies between 30 MeV and 10 GeV for the GCR spectrum, and between 30 MeV and 200 MeV for the SEP proton spectrum, we obtain neutron counting rates of $\text{GCRn} = 0.14$ per incident GCR proton and $\text{SEPN} = 0.011$ per incident SEP proton.

[29] We now use the -XLG-BP double-coincidence (DC) counting rates measured during the 31 December 2007 solar flare event by the MESSENGER NS just after the data dropout to normalize the intensities of the SEP protons (through the K factor in equation (1)) and the GCR protons. We use the fast-neutron and -XLG DC counting rates after the data dropout between about 0136 and 0330 UTC, shown in Figure 5c. We note that the DC counting rate (given by the red line in Figure 5c) before the event was $550(0.3) = 165 \text{ s}^{-1}$ and was $550(1.6) = 880 \text{ s}^{-1}$ at about 0430 UTC just after the recovery from the dropout. This yields a ratio of counting rates after the data dropout to that before the dropout of $R = (1.6-0.3)/0.3$. During the same times, the fast-neutron counting rate was $F_{\text{GCRn}} = 0.5 \text{ s}^{-1}$ and $F_{\text{SEPN}} = 1.6 \text{ s}^{-1}$, as shown by the black trace. We also note that the triple-coincidence counting rate drops to background (the blue trace in Figure 5c) after the data dropout, which is consistent with our choice of equation (1) for the SEP proton spectrum. As seen in Figure 9a, this spectrum yields

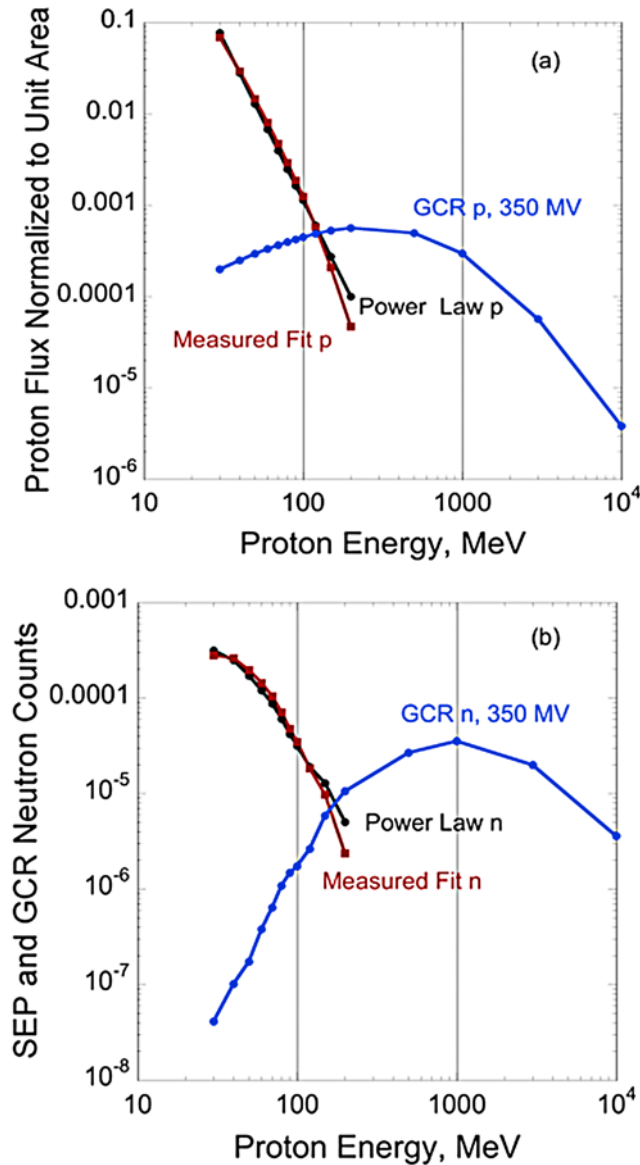


Figure 9. (a) Proton flux spectra and (b) neutron counting rates as functions of incident proton energy. The term “power law” refers to the functional form of the incident solar energetic particle proton (SEP) spectrum, here assumed to be a power law with exponent -3.5 ; the term “measured fit” refers to the form of the SEP proton spectrum given by equation (1); and GCR refers to the form given in the work of *McKinney et al.* [2006] for an assumed modulation potential of 350 MV.

a sharply dropping flux at energies greater than about 200 MeV, which is close to, but just above, the energy break between double and triple coincidences for protons incident on $-XLG$ within the cone of acceptance for a triple coincidence. Both proton spectra in Figure 9a produce nearly equal integrated neutron counting rates.

[30] We need one more factor to convert measured counting rates to the simulated neutron counting rates for purported SEP-proton-generated neutrons in the MESSENGER spacecraft. From *Sullivan* [1971, equation (11)], the geometric

factor for GCR interactions is the total isotropic solid angle, 2π , minus the triple-coincidence value, 1.26 , $G_{DC}(GCR) = [2\pi - 1.26] = 5.03$. This value must be compared with the G factor for double-coincidence SEP proton interactions, given by $G_{DC}(SEP) = \pi + (\pi - 0.628)/2 = 4.40$. We note that the SEP G factor differs from the GCR factor for two reasons. First, the full solid-angle factor along the outward normal to $-XLG$ is effective for SEPs, (π), because the SEPs are not sufficiently energetic to penetrate through all three sensors to produce a triple coincidence and, second, the part of the solid angle from the $+XLG$ side of the NS that misses $+XLG$ must be divided by 2 because the spacecraft cuts off half of the SEP protons coming from the $+XLG$ direction (see Figure 4c).

[31] Assembling all the factors, the upper limit on the neutron count rate generated by SEP protons (if all energetic particle counts are due to protons) is estimated to be:

$$\begin{aligned} \text{SEP}(\text{neutrons}) &= F_{GCRn}[R][\text{SEPn}/G_{DC}(\text{SEP})]/[GCRn/G_{DC}(GCR)], \text{ or,} \\ \text{SEP}(\text{neutrons}) &= 0.5[(1.6 - 0.3)/0.3][0.01105/4.40]/[0.135/5.03] \\ &= 0.203 \text{ s}^{-1}. \end{aligned}$$

[32] Our measured fast-neutron counting rate for the time after the dropout is $1.6 - 0.5 = 1.1 \text{ neutrons s}^{-1}$, a factor of 5.4 times greater than the estimated upper limit estimate given above for SEP-generated neutrons for the 31 December 2007 event. We note that this factor of 5.4 is a lower limit because not all observed double coincidences are due to SEP protons having energies greater than 30 MeV. We therefore conclude that most of the neutrons measured after the data dropout on 31 December 2007 must have come from the Sun.

5. Summary and Discussion

[33] In summary, a solar flare of scale M2 was observed by a host of spacecraft positioned around the Sun and also by the radio spectrometer on Bruny Island, Australia (Figures 2, 3, and 4). The flare consisted of several acceleration episodes as seen through its generation of multiple type II and III radio bursts (Figure 3). The MESSENGER particle-counting rates had a relatively sharp, energy-independent onset, and they smoothed out after several hours to a relatively quiescent decay that was characterized by a simple e -folding decay time of 2.84 h (Figure 5c). The flare had a two-ribbon structure and was also accompanied by the launching of a CME (Figure 2). Either this CME, or multiple explosively driven pressure pulses from the event, drove shocks in the upstream solar wind close to the Sun, as evidenced by the several type II bursts seen in Figure 3. The onset of energetic particles at MESSENGER closely followed the passage of a tangential discontinuity in the IMF carried by the solar wind (identified in Figure 6), which is consistent with the observed simple, sharp, energy-independent rise to maximum counting rates shown in Figure 5a. Also observed with the MESSENGER NS was an enhanced, extended flux of fast neutrons with apparent neutron energy deposited in the NS between 0.5 and 7.5 MeV as shown in Figure 5c.

[34] When we assemble all of the facts from sections 2–4, we find several lines of evidence that are most convincing for attributing a large fraction of the neutron enhancement

seen at MESSENGER after the safe-mode data dropout to neutrons from the Sun. A possible alternative explanation, which we do not think is supported by the totality of the data, is that the majority of measured fast neutrons may have been generated locally in the spacecraft from nuclear reactions owing to energetic protons hitting the spacecraft. Because of a partial failure in the MESSENGER EPS, it is not known explicitly whether the energetic particles that reached MESSENGER were electrons, ions, or both. However, at least the initial portion of the event seen by the EPS before the safe-mode data dropout must have been entirely electrons by virtue of their observed short time of flight between the Sun and MESSENGER. Because of the absence of any significant secondary positive inflection in EPS counting rates after the initiation of the data dropout that might have signaled the arrival of 65 keV to 1 MeV protons from the coronal flare site of the same event, we conclude that most of the particles detected by the EPS throughout this event were electrons. This observation does not preclude the arrival at the MESSENGER spacecraft of a relatively small flux of protons having energies higher than 1 MeV up to and beyond 120 MeV throughout the event. Regardless, we deduce that the ratio of the measured neutron count rate to the upper bound on the contribution from SEP protons estimated from the double-coincidence –XLG-BP counting rates is at least a factor of 5, as shown in section 4.

[35] Second, the energetic particle event at MESSENGER began just after passage of a tangential discontinuity (which was long after energetic electrons and 100 MeV/AMU ions could have reached MESSENGER if they were accelerated and released at the time of the flare). This occurrence is readily explained if the energetic particles originated from a spatially confined impulsive event, or a relatively short series of impulsive events, in the corona rather than at an extended interplanetary shock wave. High-energy ions accelerated at an extended shock would not be delimited in space by such a discontinuity but have been previously observed by *Mazur et al.* [2000] during impulsive events and attributed by *Giacalone et al.* [2000] to a random walk of magnetic field lines in the photosphere that start disconnected from, and then connect up to, the flare site in the corona. Such an occurrence is possible for a localized flare site in the corona but not at a longitudinally extended interplanetary shock. In support of this conclusion, MESSENGER was located at the far eastern flank of the CME, and no shock driven by the CME was seen at MESSENGER.

[36] Third, the time dependence of energetic particles at MESSENGER had a generally simple structure during its decay phase, with an e -folding decay time of 2.84 h, not of order a day and longer, as is often associated with CME-driven shock waves [*Reames*, 1999].

[37] Last, the time dependence at MESSENGER of neutron counting rates and the double- and triple-coincidence neutron-sensor counting rates that are attributable to very high-energy particles are significantly different, as discussed above. These differences make it difficult to attribute the neutron enhancement detected by the NS to the incidence of energetic protons on the MESSENGER spacecraft. These differences, in turn, argue strongly against the observed neutrons having originated from the spacecraft rather than from the Sun. However, as stated previously, we cannot rule

out the possibility that some of the neutrons detected aboard MESSENGER after the data dropout were generated by energetic protons from the flare site interacting with spacecraft material because of the similarities of their decay phases.

[38] Identification of a solar origin for the observed neutrons leads to two important conclusions. First, the fact that the event decayed over a time period of about 9 h with an e -folding time of 2.84 h argues against generation of neutrons in the chromosphere only during the short series of impulsive events evident in the cluster of type III electron bursts seen near the flare onset. The mean lifetime of a neutron is too much shorter than the 2.84 h e -folding time for this to be true. Neither can the neutrons have originated in the activity that produced the multiple peaks in the energetic electron flux seen at MESSENGER, for the same reason. We therefore conclude that neutrons during this event were produced continuously in the solar atmosphere over a period of about 9 h. Such extended production of solar flare neutrons has been reported previously for extended 2.2 MeV gamma-ray line emission from the 11 and 15 June 1991 flares [*Rank et al.*, 1996; *Ryan*, 2000, and references therein]. It is interesting to note that the decay of these gamma emissions (which come from absorption of thermal neutrons by protons just above the photosphere) were 220 ± 50 and 180 ± 100 min. These decay times are, within errors, equal to that of our extended neutron flare event, which is 2.84 h = 170 min. A simple explanation of such an occurrence is that ions were accelerated over an extended time period during the flare, stored temporarily on closed magnetic field loops high in the corona, and then lost to the chromosphere through pitch angle scattering by coronal turbulence, thereby continuously producing new neutrons as discussed in the review of long-duration solar gamma-ray flares by *Ryan* [2000].

[39] A secondary implication of this line of reasoning is that the extended corona must contain an enhanced flux of 1–8 MeV protons (and their associated beta-decay electrons with a high-energy endpoint of 783 keV). These protons and electrons are the residues of the beta decay of the 1–8 MeV neutrons that continuously stream away from the Sun during the decay of this type of flare event. These energetic protons can then function as an analog of the cosmic ray albedo neutron decay (CRAND) protons that provide an important supply of very energetic protons to the inner terrestrial radiation belt [*Selesnick et al.*, 2007]. The neutrons identified here during the 31 December 2007 flare yield the solar flare analog of terrestrial radiation-belt energetic protons that can be called flare ion neutron decay (FIND) protons. The importance here is that as solar activity picks up, we expect more of these moderate-sized solar flares, which will lead to a significant, ubiquitous population of 1–8 MeV protons in the extended corona. These protons could then become the seed population for further acceleration at CME-driven shock waves [*Tylka et al.*, 2005] to produce very large solar-energetic particle events that have been observed in near-Earth orbit and beyond [*Mewaldt*, 2006].

[40] **Acknowledgments.** The MESSENGER mission is supported by the NASA Discovery Program. We are grateful to the entire MESSENGER team for making the mission a success. Special thanks go to Brian Anderson

for his essential contributions to the Magnetometer instrument. This work was carried out under the auspices of the Planetary Science Institute, Johns Hopkins University Applied Physics Laboratory, and all of the institutions of the coauthored team. The work at Caltech was supported by NASA under grant NNX-08A111G, and W. C. Feldman also thanks the Los Alamos National Laboratory for providing an office and access to their library during parts of this project.

[41] Amitava Bhattacharjee thanks the reviewers for their assistance in evaluating this paper.

References

- Anderson, B. J., et al. (2007), The Magnetometer instrument on MESSENGER, *Space Sci. Rev.*, *131*, 417–450, doi:10.1007/s11214-007-9246-7.
- Andrews, G. B., et al. (2007), The Energetic Particle and Plasma Spectrometer on the MESSENGER spacecraft, *Space Sci. Rev.*, *131*, 523–556, doi:10.1007/s11214-007-9272-5.
- Baker, D. N., et al. (2009), Space environment of Mercury at the time of the first MESSENGER flyby: Solar wind and interplanetary magnetic field modeling of upstream conditions, *J. Geophys. Res.*, *114*, A10101, doi:10.1029/2009JA014287.
- Bougeret, J.-L., et al. (2008), S/WAVES: The radio and plasma wave investigation on the STEREO mission, *Space Sci. Rev.*, *136*, 487–528, doi:10.1007/s11214-007-9298-8.
- Erickson, W. C. (1997), The Bruny Island radio spectrometer, *Publ. Astron. Soc. Aust.*, *14*, 278–282.
- Giacalone, J., J. R. Jokipii, and J. E. Mazur (2000), Small-scale gradients and large-scale diffusion of charged particles in the heliospheric magnetic field, *Astrophys. J.*, *532*, L75–L78, doi:10.1086/312564.
- Goldsten, J. O., et al. (2007), The MESSENGER Gamma-Ray and Neutron Spectrometer, *Space Sci. Rev.*, *131*, 339–391, doi:10.1007/s11214-007-9262-7.
- Howard, R. A., et al. (2008), Sun Earth Connection Coronal and Heliospheric Investigation (SECCHI), *Space Sci. Rev.*, *136*, 67–115, doi:10.1007/s11214-008-9341-4.
- Hua, X.-M., and R. E. Lingenfelter (1987), Solar flare neutron production and angular dependence of the capture gamma-ray emission, *Sol. Phys.*, *107*, 351–383, doi:10.1007/BF00152031.
- Hua, X.-M., B. Kozlovsky, R. E. Lingenfelter, R. Ramaty, and A. Stupp (2002), Angular and energy-dependent neutron emission for solar flare magnetic loops, *Astrophys. J. Suppl. Ser.*, *140*, 563–579, doi:10.1086/339372.
- Krucker, S., and R. P. Lin (2008), Hard X-ray emissions from partially occulted solar flares, *Astrophys. J.*, *673*, 1181–1187, doi:10.1086/524010.
- Lawrence, D. J., W. C. Feldman, J. O. Goldsten, and S. C. Solomon (2009), Identification of neutron absorbing elements on Mercury's surface using MESSENGER neutron data, *Lunar Planet. Sci.*, *XL*, Abstract 1761.
- Leary, J. C., et al. (2007), The MESSENGER spacecraft, *Space Sci. Rev.*, *131*, 187–217, doi:10.1007/s11214-007-9269-0.
- Lin, R. P., et al. (2002), The Reuven Ramaty High-Energy Solar Spectroscopic Imager (RHESSI), *Sol. Phys.*, *210*, 3–32, doi:10.1023/A:1022428818870.
- Lin, R. P., et al. (2003), RHESSI observations of particle acceleration and energy release in an intense solar gamma-ray line flare, *Astrophys. J.*, *595*, L69–L76, doi:10.1086/378932.
- Liu, Y., J. G. Luhmann, S. D. Bale, and R. P. Lin (2009), Relationship between a coronal mass ejection-driven shock and a coronal metric type II burst, *Astrophys. J.*, *691*, L151–L155, doi:10.1088/0004-637X/691/2/L151.
- Masuda, S., T. Kosugi, H. Hara, S. Tsuneta, and Y. Ogawa (1994), A loop-top hard X-ray source in a compact solar flare as evidence for magnetic reconnection, *Nature*, *371*, 495–497, doi:10.1038/371495a0.
- Mazur, J. E., G. M. Mason, J. R. Dwyer, J. Giacalone, J. R. Jokipii, and E. C. Stone (2000), Interplanetary magnetic field line mixing deduced from impulsive solar flare particles, *Astrophys. J.*, *532*, L79–L82, doi:10.1086/312561.
- McKinney, G. W., D. J. Lawrence, T. H. Prettyman, R. C. Elphic, W. C. Feldman, and J. J. Hagerty (2006), MCNPX benchmark for cosmic ray interactions with the Moon, *J. Geophys. Res.*, *111*, E06004, doi:10.1029/2005JE002551.
- Mewaldt, R. A. (2006), Solar energetic particle composition, energy spectra, and space weather, *Space Sci. Rev.*, *124*, 303–316, doi:10.1007/s11214-006-9091-0.
- Miller, J. A., P. J. Cargill, E. A. Gordon, G. D. Holman, B. R. Dennis, T. N. LaRosa, R. M. Winglee, S. G. Benka, and S. Tsuneta (1997), Critical issues for understanding particle acceleration in impulsive solar flares, *J. Geophys. Res.*, *102*, 14,631–14,660.
- Murphy, R. J., B. Kozlovsky, G. H. Share, X.-M. Hua, and R. E. Lingenfelter (2007), Using gamma-ray and neutron emission to determine solar flare accelerated particle spectra and composition and the conditions within the flare magnetic loop, *Astrophys. J. Suppl. Ser.*, *168*, 167–194, doi:10.1086/509637.
- Nieto, M. M., W. C. Feldman, and D. J. Lawrence (2008), Testing the unitarity of the CKM matrix with a space-based neutron decay experiment, *Mod. Phys. Lett. A*, *23*, 1735–1743, doi:10.1142/S0217732308027187.
- Pelowitz, D. B. (Ed.) (2005), *MCNPX User's Manual Version 2.5.0, Rep. LA-CP-05-0369*, Los Alamos Natl. Lab., Los Alamos, N. M.
- Rank, G., K. Bennett, H. Bloemen, H. Debrunner, J. Lockwood, M. McConnell, J. Ryan, V. Schönfelder, and R. Suleiman (1996), Extended gamma-ray emission in solar flares, *AIP Conf. Proc.*, *374*, 219–224.
- Reames, D. V. (1999), Particle acceleration at the Sun and in the heliosphere, *Space Sci. Rev.*, *90*, 413–491, doi:10.1023/A:1005105831781.
- Ryan, J. M. (2000), Long-duration solar gamma-ray flares, *Space Sci. Rev.*, *93*, 581–610, doi:10.1023/A:1026547513730.
- Schlemm, C. E., II, et al. (2007), The X-Ray Spectrometer on the MESSENGER spacecraft, *Space Sci. Rev.*, *131*, 393–415, doi:10.1007/s11214-007-9248-5.
- Selesnick, R. S., M. D. Looper, and R. A. Mewaldt (2007), A theoretical model of the inner proton radiation belt, *Space Weather*, *5*, S04003, doi:10.1029/2006SW000275.
- Solomon, S. C., R. L. McNutt Jr., R. E. Gold, and D. L. Domingue (2007), MESSENGER mission overview, *Space Sci. Rev.*, *131*, 3–39, doi:10.1007/s11214-007-9247-6.
- Sullivan, J. D. (1971), Geometrical factor and directional response of single and multi-element particle telescopes, *Nucl. Instrum. Methods*, *95*, 5–11, doi:10.1016/0029-554X(71)90033-4.
- Tylka, A. J., C. M. S. Cohen, W. F. Dietrich, M. A. Lee, C. G. MacLennan, R. A. Mewaldt, C. K. Ng, and D. V. Reames (2005), Shock geometry, seed populations, and the origin of variable elemental composition at high energies in large gradual solar particle events, *Astrophys. J.*, *625*, 474–495, doi:10.1086/429384.

D. N. Baker, Laboratory for Atmospheric and Space Physics, University of Colorado, Boulder, CO 80303, USA.

W. C. Feldman, Planetary Science Institute, 1700 East Fort Lowell, Suite 106, Tucson, AZ 85719, USA. (feldman@psi.edu)

R. E. Gold, J. O. Goldsten, D. K. Haggerty, G. C. Ho, D. J. Lawrence, and E. A. Rhodes, Johns Hopkins University Applied Physics Laboratory, Laurel, MD 20723, USA.

S. Krucker and R. P. Lin, Space Sciences Laboratory, Physics Department, University of California, Berkeley, CA 94720, USA.

R. A. Mewaldt, Physics Department, California Institute of Technology, Pasadena, CA 91125, USA.

R. J. Murphy and A. Vourlidas, Naval Research Laboratory, Washington, DC 20375, USA.

L. R. Nittler and S. C. Solomon, Department of Terrestrial Magnetism, Carnegie Institution of Washington, Washington, DC 20015, USA.

J. A. Slavin, NASA Goddard Space Flight Center, Code 670, Greenbelt, MD 20771, USA.

R. D. Starr, Department of Physics, Catholic University of America, Washington, DC 20064, USA.

F. Vilas, MMT Observatory, University of Arizona, Tucson, AZ 85721, USA.